

Echoes of charged black-bounce spacetimes

shurui Wu ^a, Z. W. Long ^b, Dong Liu, and Yi Yang
College of Physics, Guizhou University, Guiyang, 550025, China.
(Dated: February 1, 2022)

In present work, the evolution of scalar field and electromagnetic field under the background of the charged black-bounce spacetimes are investigated, and we obtain an obvious echoes signal which appropriately reports the properties of the charged black-bounce spacetimes and disclose the physical reasons behind such phenomena. Furthermore, by studying the quasinormal ringdown, we analyze the three states of the charged black-bounce spacetimes in detail, our results show that the echoes signal only appears when ($|Q| \leq m$) and ($|l| > m + \sqrt{m^2 - Q^2}$) in this spacetime, while when the parameters demand ($|Q| > m$), the echoes signal will be transformed into a quasinormal ringdown of the two-way traversable wormhole, and the charged black-bounce is a regular black hole with normal horizons by requiring ($|Q| \leq m$) and ($|l| < m - \sqrt{m^2 - Q^2}$).

I. INTRODUCTION

In recent years, the first measurements of the shadow image captured by Event Horizon Telescope (EHT) [1–6] and the gravitational wave (GW) searches by the LIGO Scientific and Virgo collaboration for the merger of compact binaries [7–10] energized physicists in black hole physics, as the most extremely compact objects characterized by the existence of event horizons, black holes are some of the most important models in GW observations. In particular, GW echoes from black holes can help us to study the properties of the compact object itself, and moreover, probably furnish an avenue to the nature of quantum gravity. The notion of GW echoes was proposed in the context of the GW ringdown signals, aiming to study the phenomena in the vicinity of the black holes and their exotic compact alternatives.

On the other hand, as the characteristic sound of black holes, the quasinormal models (QNMs) are dominantly governed by the spacetimes in the vicinity of the horizon. It is well known that once a black hole is perturbed [11], there are three stages that are responsible for the perturbations evolution in time. The first one is a relatively short period of initial outburst of radiation, the second one is a usually long period of damping proper oscillations which dominated by the QNM, and the third one is the power-law tail. Here, we focus on the second stage of the evolution of perturbations represented by QNM. By analyzing black hole perturbation equations, one can derive the QNMs, and the potential solution is expressed by the pure ingoing wave at the event horizon and the pure outgoing wave at infinity [12, 13]. Moreover, by studying the black hole QNMs, we can disclose the frequencies of QNMs [14, 15], which are not only related to the basic physical properties of the black hole but also may provide reliable evidence of the existence of the black holes [16]. The QNMs of wormholes have drawn much attention. Poulami Dutta Roy et al [17] studied a family of ultra-static Lorentzian wormholes and obtained the scalar QNMs, their results may be used as a template for further studies on the gravitational wave physics of exotic compact objects; in Ref.[18], they studied the phantom wormholes and observe obvious signals of echoes, their results showed that the dark energy equation of state has a clear imprint in echoes in wave perturbations; M.S.Churilova et al[19] studied the QNM of regular black-hole/wormhole transition and obtained unique wormhole echoes picture near the threshold, their results showed that different parameters corresponding to different spacetime, and only the traversable wormhole spacetime background has a clear echo picture. In addition, more related works can be seen in Refs.[20–27].

Recently, various aspects of the charged black-bounce spacetimes have been proposed, which are the Reissner Nordström geometry [28, 29]. In this paper, we attempt to provide an investigation to the QNM of the charged black-bounce spacetimes and disclose the physical reasons behind such phenomena. Physically, we analyse the properties of spacetimes in the context of the perturbation of electromagnetic fields and scalar fields, and our results show that echoes signal appears on the condition that the parameters are constrained.

The paper is organized as follows. In Sec.II, we introduce the charged black-bounce spacetimes, the equations of motion under the influence of scalar field and electromagnetic field perturbation, meanwhile the corresponding effective potential are derived and the figure of the effective potential under the perturbation of electromagnetic field is discussed. In Sec.III, the time domain integration method is introduced. In Sec.IV, the time-domain profiles of the electromagnetic field and scalar field in the context of the black hole and the wormhole by configuring different spacetime parameters are analyzed, including the different ringdown behaviors. In Sec.V, the QNM frequencies of the charged black-bounce spacetimes are reported. Finally, the work is summarized in Sec.VI.

^a 2454016392@qq.com.

^b Corresponding author:zwlong@gzu.edu.cn.

II. SCALAR FIELD AND ELECTROMAGNETIC FIELD PERTURBATION IN THE CHARGED BLACK-BOUNCE SPACETIMES

We introduce the charged black-bounce spacetimes, its metric is given by [28–30]

$$ds^2 = -A(r)dt^2 + A^{-1}(r)dr^2 + (r^2 + l^2)d\Omega^2, \quad (1)$$

$$A(r) = 1 - \frac{2m}{\sqrt{r^2 + l^2}} + \frac{Q^2}{r^2 + l^2}, \quad (2)$$

with m being the mass of black hole, $r \in (-\infty, +\infty)$ and $d\Omega^2$ represents the line element of a unit 2-sphere. It should be noted that different parameters correspond to different spacetimes, (a) the traversable wormhole: ($|Q| \leq m$) and ($|l| > m + \sqrt{m^2 - Q^2}$); (b) the two-way traversable wormhole: ($|Q| > m$); (c) the regular black hole: ($|Q| \leq m$) and ($|l| < m - \sqrt{m^2 - Q^2}$). Furthermore, the horizons are located at

$$r_H = S_1 \sqrt{(m + S_2 \sqrt{m^2 - Q^2})^2 - l^2}, \quad (3)$$

where $S_1 = S_2 = \pm 1$, in particularly, $S_1 = 1$ corresponds to our universe, $S_1 = -1$ labels the copy of our universe, $S_2 = 1$ indicates outer horizon and $S_2 = -1$ inner horizon, respectively.

The general covariant K-G equation of scalar field can be expressed as

$$\frac{1}{\sqrt{-g}} \partial_\mu (\sqrt{-g} g^{\mu\nu} \partial_\nu \Psi) = 0, \quad (4)$$

and the motion equation of an electromagnetic field is given by

$$\frac{1}{\sqrt{-g}} \partial_\mu (F_{\rho\sigma} g^{\rho\nu} g^{\sigma\mu} \sqrt{-g}) = 0, \quad (5)$$

with $F_{\rho\sigma} = \partial_\rho A^\sigma - \partial_\sigma A^\rho$, A^μ is an electromagnetic four-potential.

According to the line elements of the charged black-bounce spacetimes, we transform the KG equation into

$$\frac{d^2 \Psi_b}{dr_*^2} + (\omega^2 - V_b(r)) \Psi_b = 0, \quad (6)$$

with $b = 0$ corresponds to scalar field, $b = 1$ to electromagnetic field, and the tortoise coordinate r_* is given by

$$dr_* = \frac{dr}{1 - \frac{2m}{\sqrt{r^2 + l^2}} + \frac{Q^2}{r^2 + l^2}}, \quad (7)$$

and for the perturbation of the scalar field and electromagnetic field, the effective potentials of the equation of motion are

$$V_0 = -r^2 A^2 (r^2 + l^2)^{-2} + Ar [2mr (r^2 + l^2)^{-\frac{3}{2}} - 2rQ^2 (r^2 + l^2)^{-2}] (r^2 + l^2)^{-1} + A^2 (r^2 + l^2)^{-1} + \frac{Al_0(l_0 + 1)}{r^2 + l^2}, \quad (8)$$

and

$$V_1 = \frac{A}{r^2 + l^2} l_0 (l_0 + 1). \quad (9)$$

Fig.1-Fig.5 report that the effective potentials change with different parameters. In Fig.1, the value of parameters satisfy the conditions of $|Q| \leq m$ and ($|l| < m - \sqrt{m^2 - Q^2}$), so Fig.1 is the effective potentials of regular black hole, which show that the maximum value of the effective potential reveal no significant changes when we remain the constant charge parameter Q and set the changeable bounce parameter l , while if we remain the constant bounce parameter l and set the changeable charge parameter Q , the maximum values of the effective potential will increase

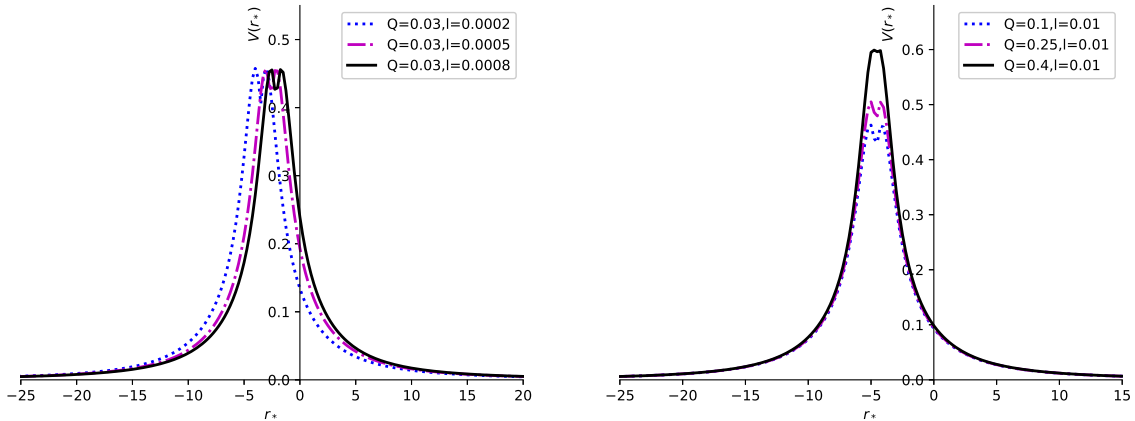


FIG. 1. The effective potentials as a function of tortoise coordinate r_* for perturbations of the electromagnetic field on the regular black hole spacetime with $m = 0.5$, $l_0 = 1$.

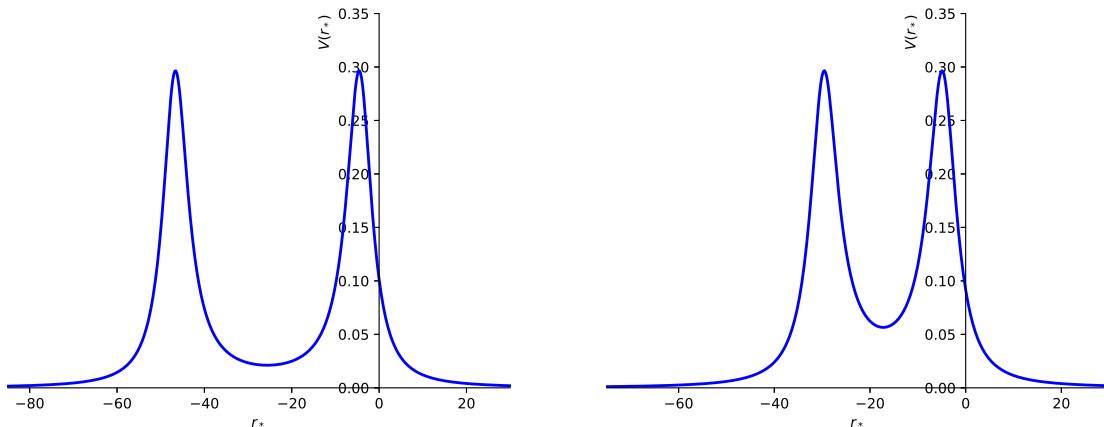


FIG. 2. The effective potentials as a function of tortoise coordinate r_* for perturbations of the electromagnetic field on the traversable wormhole spacetime with $m = 0.5$, $l_0 = 1$, $Q = 0.03$, $l = 1.01$, (left panel) $l = 1.03$ (right panel).

with the charge parameter Q . In Fig.2-Fig.4, the value of parameters satisfy the conditions of ($|Q| \leq m$) and ($|l| > m + \sqrt{m^2 - Q^2}$), so Fig.2-Fig.4 are corresponding to the traversable wormhole. Fig.2-Fig.3 show that the effective potential has obvious double peaks, and with the increasing parameter l , the double peaks will eventually merge to a single peak. In particular, Fig.4 shows that if we remain the constant bounce parameter l , the maximum value of the effective potential will increase with the charge parameter Q , and meanwhile the width of the two peaks become smaller. In Fig.5, the value of parameters satisfy the conditions of $|Q| > m$, therefore the charged black-bounce spacetimes will transform into the two-way traversable wormhole, we can see that if remaining the constant charge parameter Q , the maximum values of the effective potential decrease with the bounce parameter l , while if we remain the constant bounce parameter l , the maximum value of the effective potential increase with the charge parameter Q .

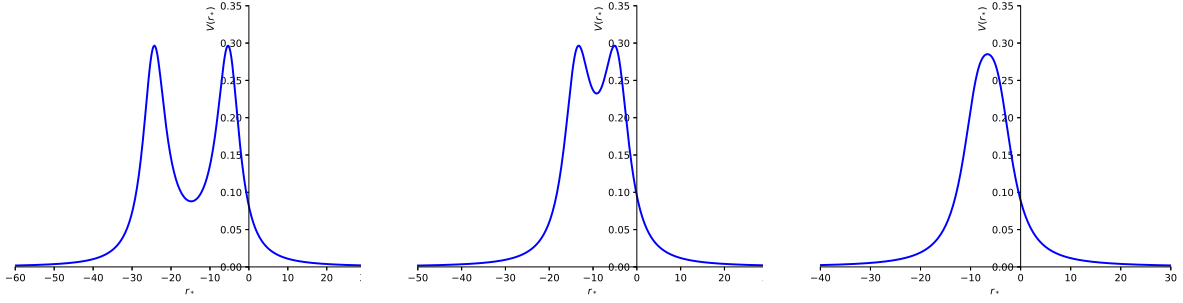


FIG. 3. The effective potentials as a function of tortoise coordinate r_* for perturbations of the electromagnetic field on the traversable wormhole spacetime with $m = 0.5$, $l_0 = 1$, $Q = 0.03$, $l = 1.05$, (left panel), $l = 1.2$, (center panel), $l = 1.7$ (right panel) .

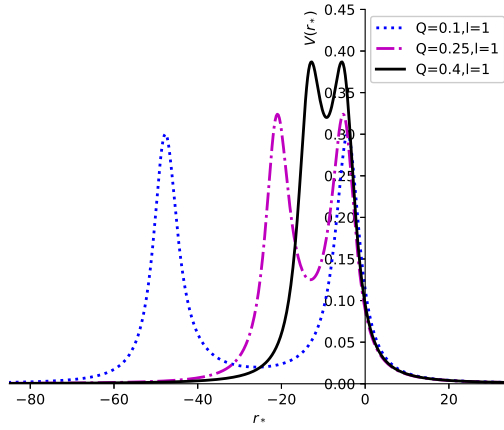


FIG. 4. The effective potentials as a function of tortoise coordinate r_* for perturbations of the electromagnetic field on the traversable wormhole spacetime with $m = 0.5$, $l_0 = 1$.

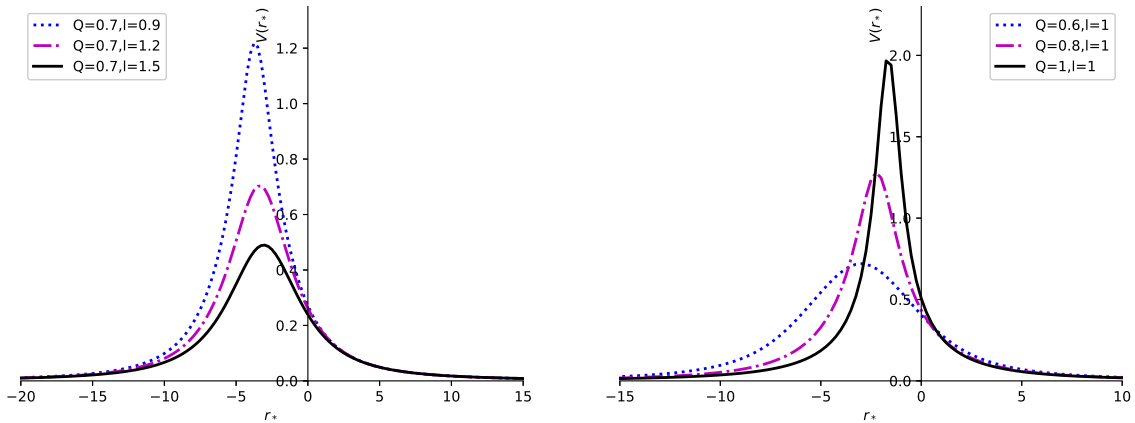


FIG. 5. The effective potentials as a function of tortoise coordinate r_* for perturbations of the electromagnetic field on the two-way traversable wormhole spacetime with $m = 0.5$, $l_0 = 1$.

III. THE TIME DOMAIN INTEGRATION METHOD

In this part, we introduce the time domain integration method. If one use the second derivative in time instead of stationary ansatz $\Phi \sim e^{-i\omega t}$ leading to ω^2 , the corresponding wave equation in the time domain can be used. We will integrate the wave equation Eq.(6) rewritten in terms of the light-cone variables $u = t - r_*$ and $v = t + r_*$, where u and v are integral constants. The appropriate discretization scheme [33, 34] is

$$\Psi(N) = \Psi(W) + \Psi(E) - \Psi(S) - \Delta^2 \frac{V(W)\Psi(W) + V(E)\Psi(E)}{8} + O(\Delta^4), \quad (10)$$

where the following designations for the points were used: $N = (u + \Delta, v + \Delta)$, $W = (u + \Delta, v)$, $E = (u, v + \Delta)$ and $S = (u, v)$. In addition, the initial data are expressed on the null surfaces $u = u_0$ and $v = v_0$. In order to facilitate the extraction of the quasinormal frequencies, we will employ the Prony method[23, 35] which helps us to fit the signal by a sum of exponents with some excitation factors.

IV. THE PICTURES OF ECHOES FOR THE CHARGED BLACK-BOUNCE SPACETIMES

In this section, we concentrate on the time evolution under the perturbations of massless scalar field and electromagnetic field in the charged black-bounce spacetimes.

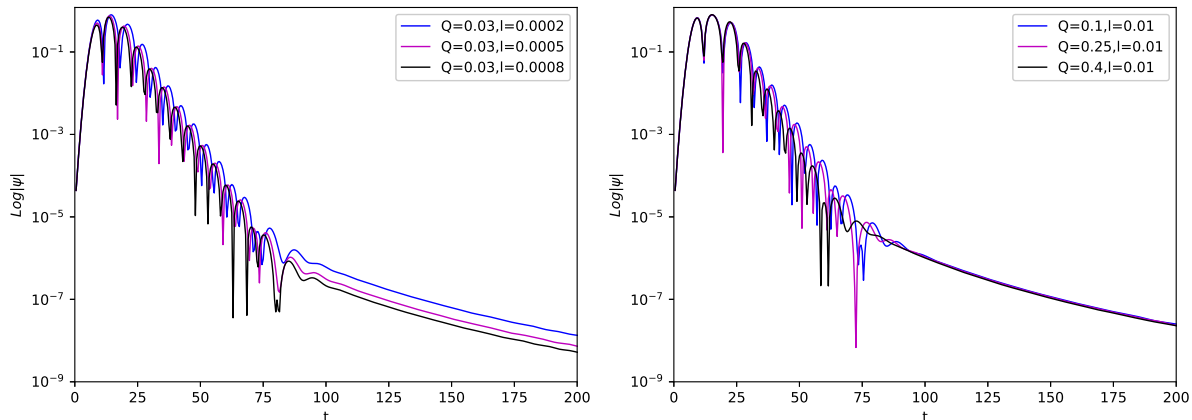


FIG. 6. Time evolution of regular black hole (left panel:the constant charge parameter Q and the changeable bounce parameter l) and (right panel:the constant bounce parameter l and the changeable charge parameter Q)with $m = 0.5$, $l_0 = 1$.

Fig.6 expresses the time evolution of regular black hole with the different spacetime parameters, which shows that there are three stages instead of echo signal. Moreover, we find that the quasinormal ringdown of regular black hole will decay slighter slower with the decreasing bounce parameter l , while it will decay faster with the increasing Q .

Fig.7-Fig.9 show electromagnetic perturbations of the charged black-bounce spacetimes for the case of ($|Q| \leq m$) and ($|l| > m + \sqrt{m^2 - Q^2}$), these pictures present the following characteristics:

(1) In terms of the values of the bounce parameter l and the charge parameter Q , the effective potentials (Fig.2 and Fig.4) express two relatively distant peaks. This phenomenon causes modification of the signal at the late times labeled as echoes, which may generate either because of the modification of the black hole metric in the vicinity of its event horizon[36, 37], or by reason of the matter situated at some distance from the compact object[38, 39]. After the black hole/wormhole transition, we find the quasinormal ringdown of the initial black hole followed by a series of echoes ($t < 100$) in Fig.7 and Fig.9 (only the red line and the blue line).

(2) When the bounce parameter l and the charge parameter Q become larger respectively, the amplitudes of the echoes signal only slightly change (Fig.7), this result is probably due to the corresponding potential function. We can see that as the parameter l and Q increase respectively, the peak value of the potential well only slightly change(Fig.2). It is because the potential well strongly constrain the scalar wave or electromagnetic wave that the echoes are generated. So almost the same height potential wells have the almost the same probability for the scalar wave or electromagnetic wave escaping from the potential well, this is also the reason why the amplitudes of the echoes signal remain almost unchanged.

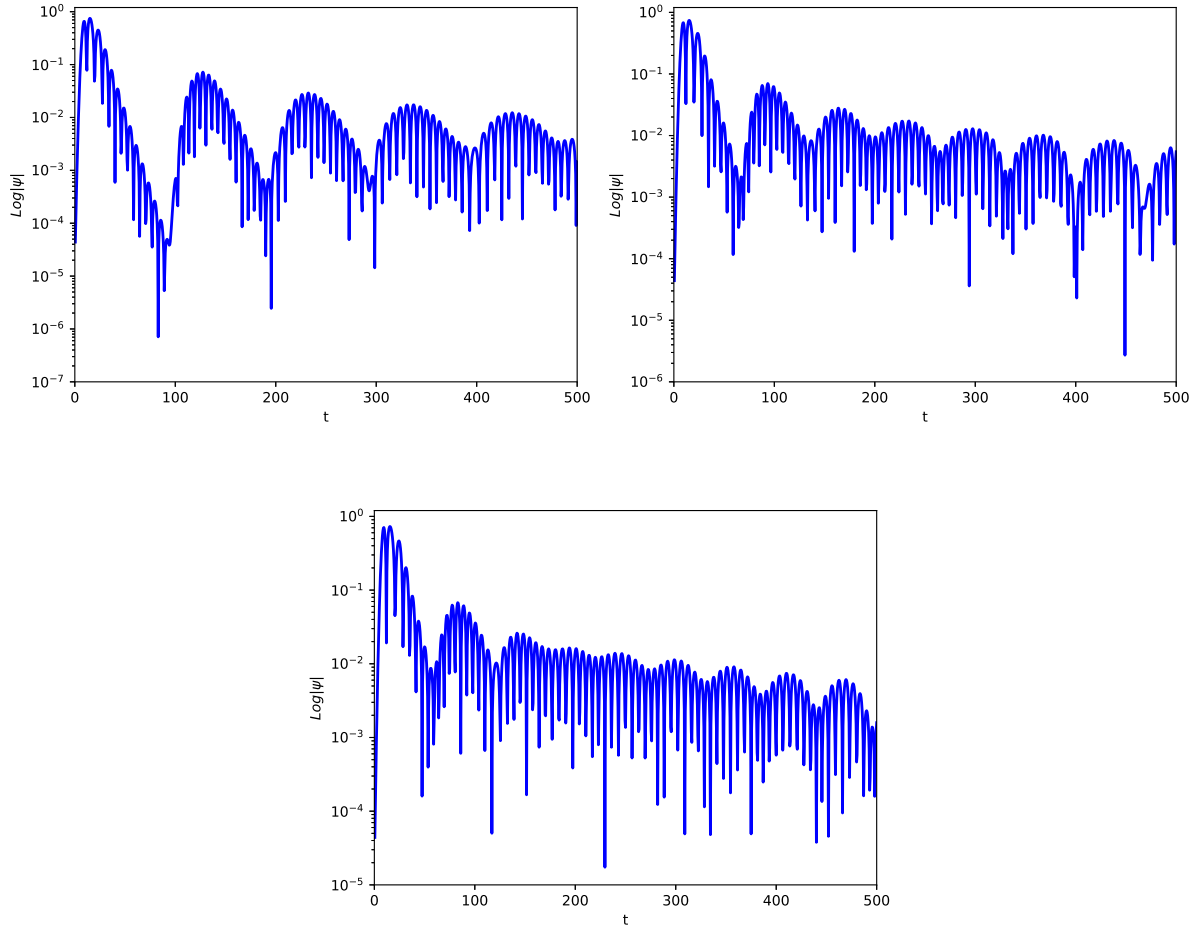


FIG. 7. Time evolution of the traversable wormhole (left panel: $l = 1.01$), (center panel: $l = 1.03$) and (right panel: $l = 1.05$) with $m = 0.5$, $l_0 = 1$.

(3) From Fig.7 to Fig.9, we can see that as the bounce parameter l and the charge parameter Q increase respectively, both peaks of the effective potential become closer and the echo effect decreases rather quickly, and the wormhole still remains a distinctive quasinormal mode. Moreover, from Fig.8 and Fig.9(black line), we find that the time evolution of the traversable wormhole have a kind of the initial outburst and obvious quasinormal mode of the wormhole spacetime.

Besides, Fig.10 shows the time evolution of the two-way traversable wormhole 's quasinormal ringing with different spacetime parameters. We can see that when remaining the constant charge parameter Q , the two-way traversable wormhole's quasinormal ringing will decay slower with the increasing bounce parameter l (left panel), while when remaining the constant bounce parameter l , the two-way traversable wormhole 's quasinormal ringing will decay faster with the increasing charge parameter Q (right panel). In fact, these results can be predicted from the corresponding pictures of the effective potentials.

From Fig.13 and Fig.15(the red line and the blue line), we show the effective potential and the semi-logarithmic plot of time evolution of scalar perturbations for the charged black-bounce spacetimes with different spacetime parameters, analogy to the case of the electromagnetic field perturbations, the echoes signal only appears when ($|Q| \leq m$) and ($|l| > m + \sqrt{m^2 - Q^2}$), and from Fig.11 to Fig.16, we can see that the effect of the changable spacetime parameters for the effective potential and the time evolution under the background of the scalar field perturbations is almost the same with the background of the electromagnetic field perturbation. But as the bounce parameter l and the charge parameter Q increase respectively, compare with the case of the electromagnetic field perturbations, the time interval between the echoes of the scalar perturbations becomes slighter shorter.

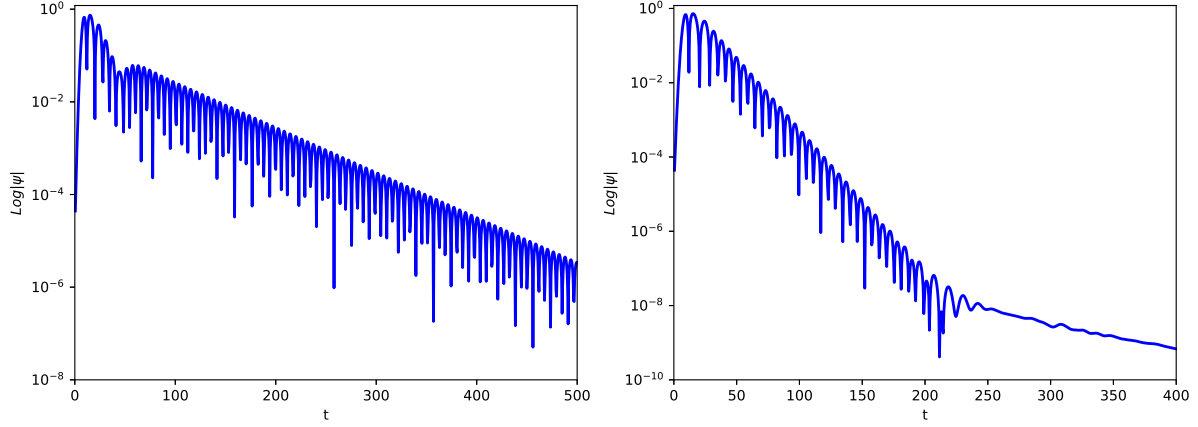


FIG. 8. Time evolution of the traversable wormhole (left panel: $l = 1.2$) and (right panel: $l = 1.7$) with $m = 0.5$, $l_0 = 1$.

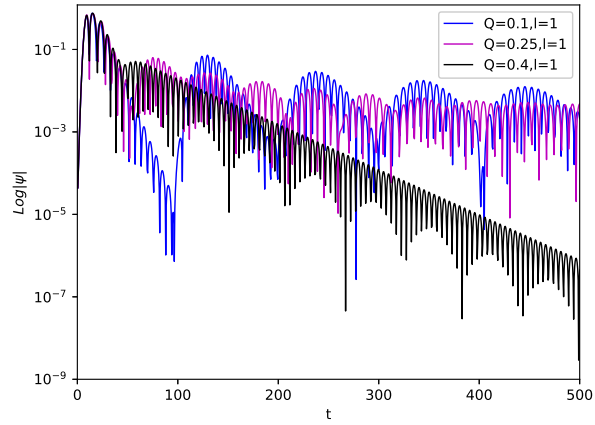


FIG. 9. Time evolution of the traversable wormhole (the constant bounce parameter l and the changeable charge parameter Q) with $m = 0.5$, $l_0 = 1$.

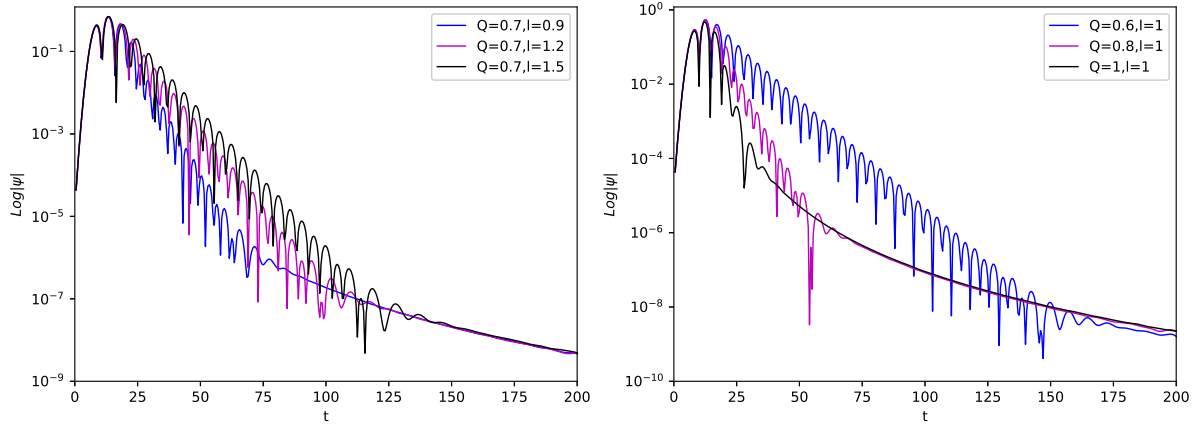


FIG. 10. Time evolution of the two-way traversable wormhole (left panel: the constant charge parameter Q and the changeable bounce parameter l) and (right panel: the constant bounce parameter l and the changeable charge parameter Q) with $m = 0.5$, $l_0 = 1$.

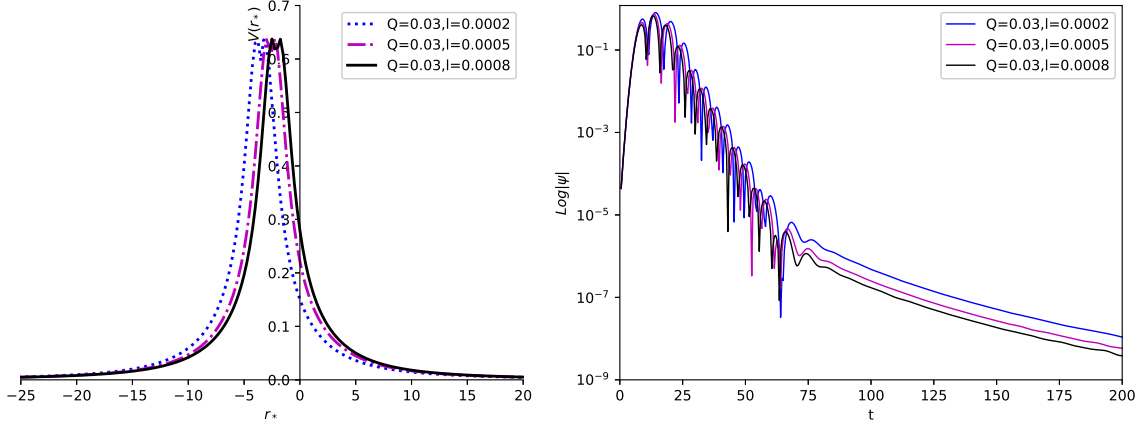


FIG. 11. The effective potential (left panel) and the semi-logarithmic plot of time evolution of scalar perturbations (right panel) for the regular black hole with $m = 0.5$, $l_0 = 1$.

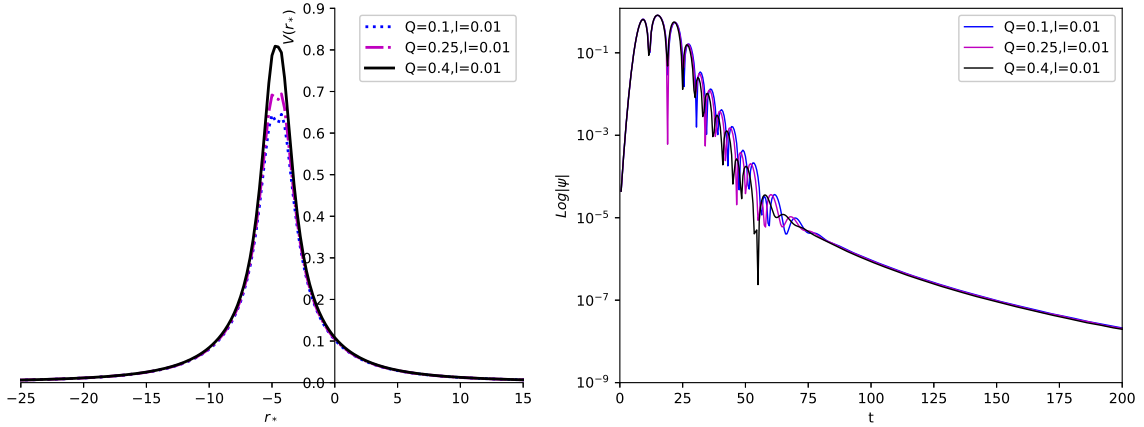


FIG. 12. The effective potential (left panel) and the semi-logarithmic plot of time evolution of scalar perturbations (right panel) for the regular black hole with $m = 0.5$, $l_0 = 1$.

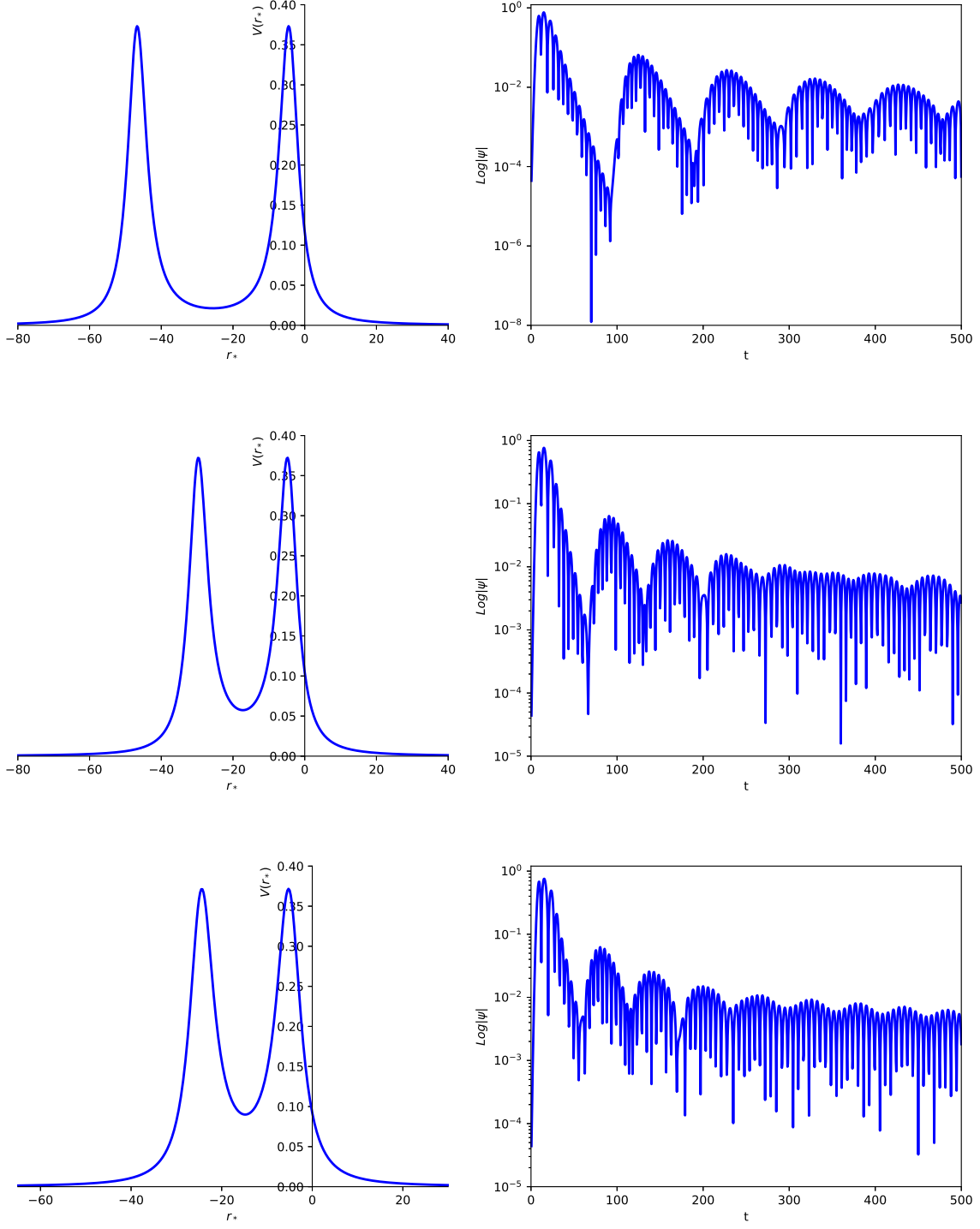


FIG. 13. The effective potential (left panel) and the semi-logarithmic plot of time evolution of scalar perturbations (right panel) with $Q = 0.03$ and $l = 1.01$, $l = 1.03$, $l = 1.05$ (from top to bottom) for the traversable wormhole with $m = 0.5$, $l_0 = 1$.

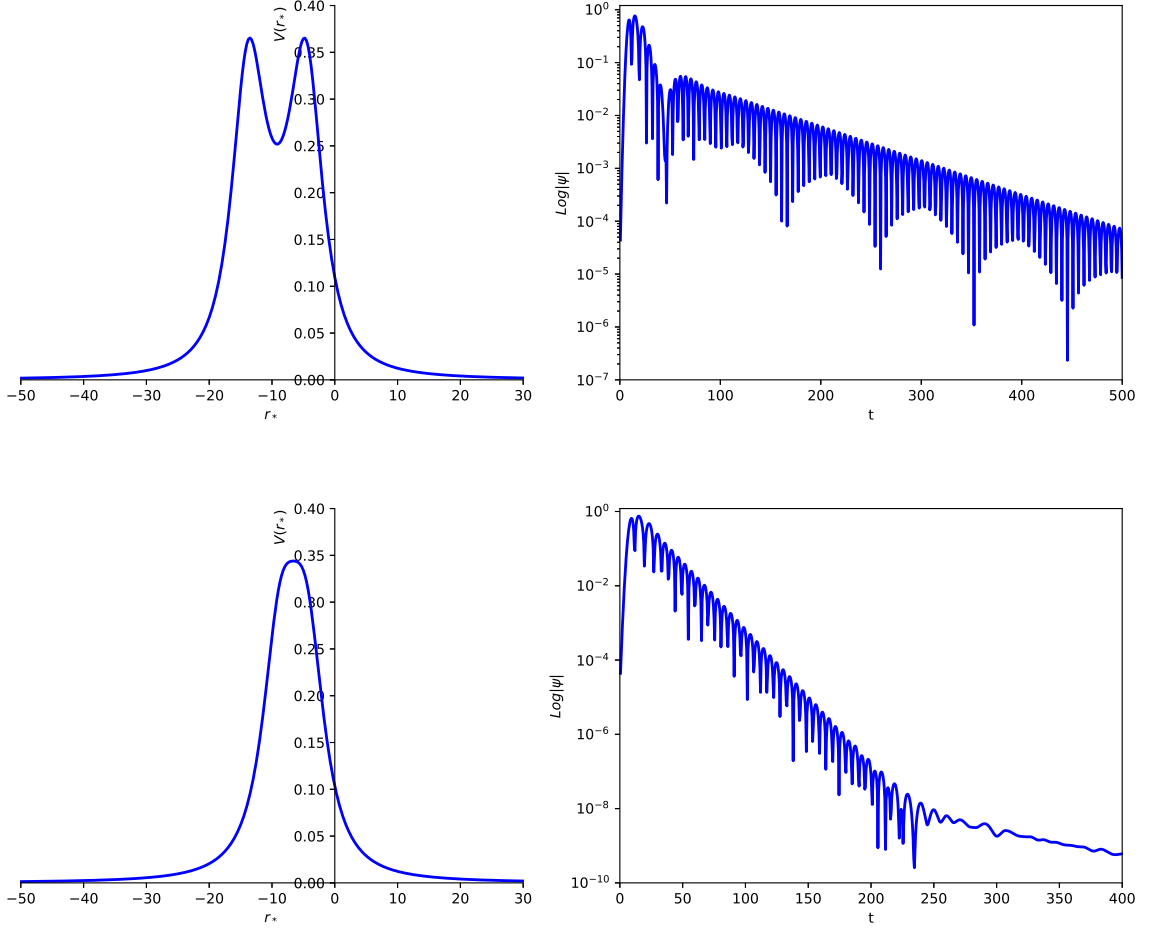


FIG. 14. The effective potential (left panel) and the semi-logarithmic plot of time evolution of scalar perturbations (right panel) with $Q = 0.03$ and $l = 1.2, l = 1.7$ (from top to bottom) for the traversable wormhole with $m = 0.5, l_0 = 1$.

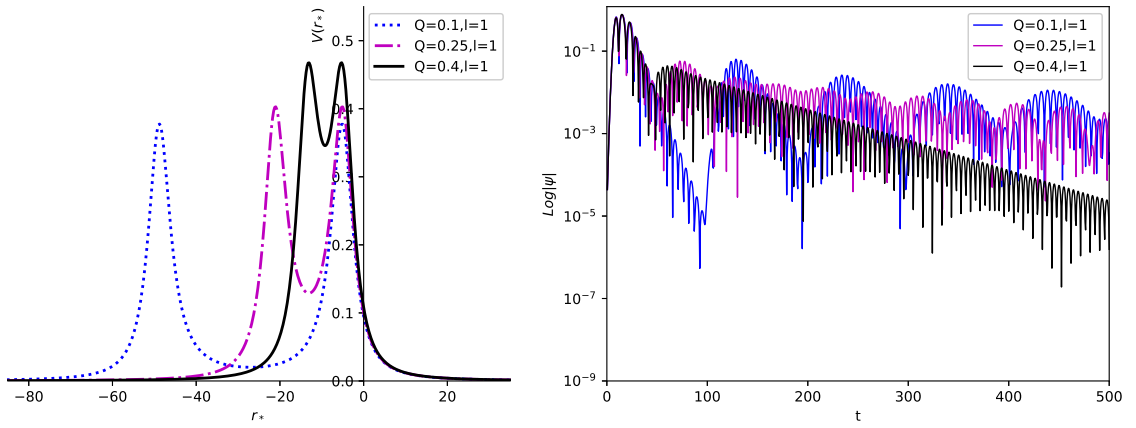


FIG. 15. The effective potential (left panel) and the semi-logarithmic plot of time evolution of scalar perturbations (right panel) for the traversable wormhole with $m = 0.5, l_0 = 1$.

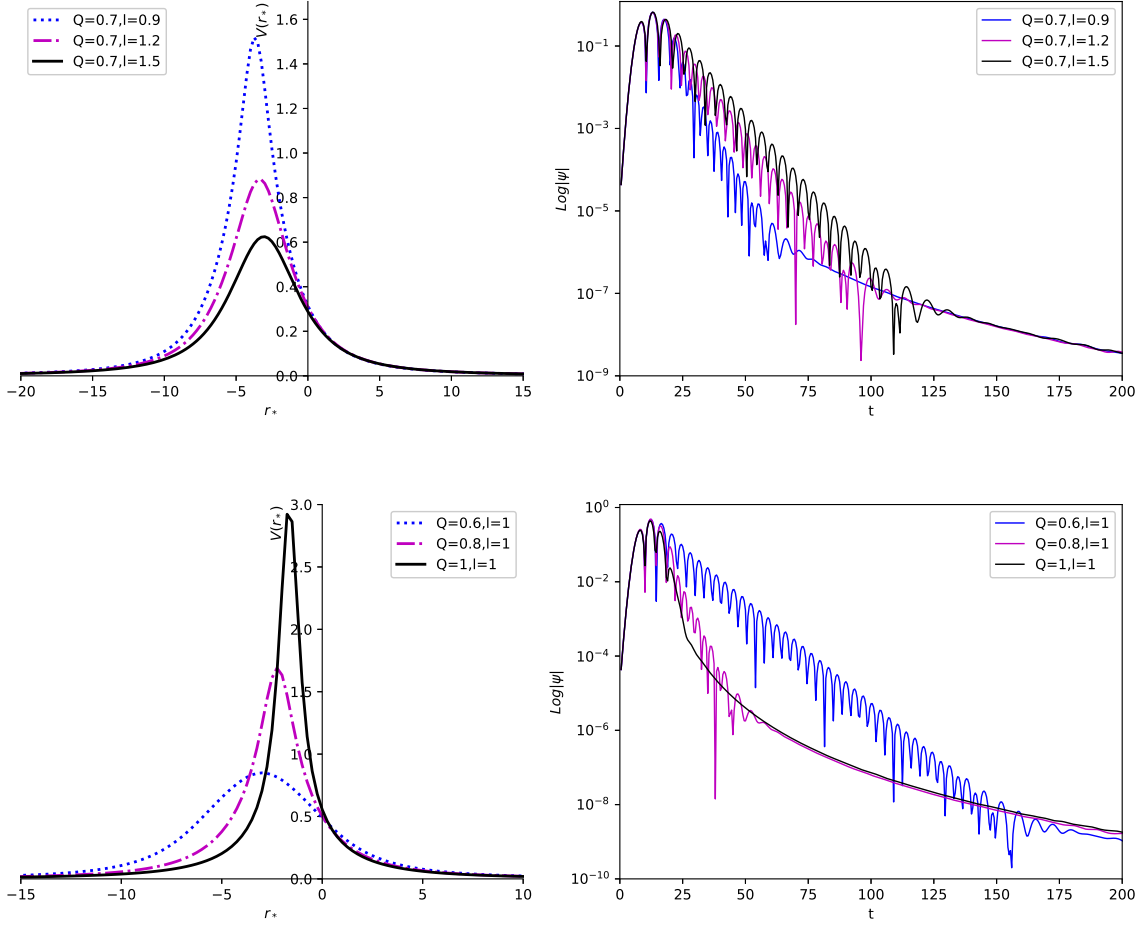


FIG. 16. The effective potential (left panel) and the semi-logarithmic plot of time evolution of scalar perturbations (right panel) for the two-way traversable wormhole with $m = 0.5$, $l_0 = 1$.

V. THE QNM FREQUENCIES OF THE CHARGED BLACK-BOUNCE SPACETIMES

In this section, we will study the time domain profiles of the charged black-bounce spacetimes, as the introduction in Sec.III, the Prony method is used for extracting the QNM frequencies. We list the QNM frequencies of the charged black-bounce spacetimes in terms of the different bounce parameter l and different charge parameter Q . It should be noted that the extraction of frequencies from the profiles obtained with the help of time domain integration strongly depends on the temporal range which is determined to be the quasinormal ringing, so in order to have a better comparison with the frequencies under different parameters, we set the almost same temporal range. The table presents the following three characteristics:

- (1) For the case of the regular black hole, as the bounce parameter l and the charge parameter Q increase respectively, the damping rate is also increasing, this result verifies the properties of the Fig.6, Fig.11 and Fig.12.
- (2) For the case of the traversable wormhole, as the bounce parameter l and the charge parameter Q increase respectively, the real part of the QNM frequencies is increasing, while the imaginary part of the QNM frequencies is decreasing.
- (3) For the case of the two-way traversable wormhole, for the smaller bounce parameter l , perturbation decays are faster, while for the bigger charge parameter Q , the perturbation decays are faster, this result verifies the properties of the Fig.10 and Fig.16.

TABLE . The fundamental quasinormal mode for the charged black-bounce spacetimes

	the scalar field	the electromagnetic field
the regular black hole		
	$l=0$ 0.680509-0.216229i	0.578712-0.179554i
$Q=0.03$	$l=0.0002$ 0.730913-0.251657i	0.618788-0.210352i
	$l=0.0005$ 0.732307-0.252514i	0.619427-0.212101i
	$l=0.0008$ 0.732193-0.253059i	0.61961-0.21216i
	$Q=0.1$ 0.733064-0.245774i	0.626881-0.20534i
$l=0.01$	$Q=0.25$ 0.758074-0.257198i	0.649738-0.216194i
	$Q=0.4$ 0.80371-0.281667i	0.693411-0.240937i
the traversable wormhole		
	$l=1.01$ 0.57998-0.138985i,echo	0.518216-0.128396i,echo
	$l=1.03$ 0.581143-0.135181i,echo	0.520363-0.125905i,echo
$Q=0.03$	$l=1.05$ 0.583718-0.131175i,echo	0.522778-0.123967i,echo
	$l=1.2$ 0.642162-0.115745i,0.574236-0.0149152i	0.527911-0.0964915i,0.539504-0.0223807i
	$l=1.7$ 0.602112-0.0836229i	0.539384-0.0886517
	$Q=0.1$ 0.588552-0.135442i,echo	0.519173-0.129354i,echo
$l=1$	$Q=0.25$ 0.605438-0.130555i,echo	0.546706-0.12292i,echo
	$Q=0.4$ 0.650319-0.0962773i,0.660092-0.0169932i	0.583465-0.0869669i,0.62293-0.0252696i
the two-way traversable wormhole		
	$l=0.9$ 0.807521-0.356207i	1.03615-0.238898i
$Q=0.7$	$l=1.2$ 0.903813-0.185995i	0.799599-0.178136i
	$l=1.5$ 0.761068-0.162117i	0.668494-0.153286i
	$Q=0.6$ 0.914065-0.126436i	0.837055-0.132897i
$l=1$	$Q=0.8$ 1.18335-0.338934i	1.03316-0.299633i
	$Q=1$ —	—

VI. CONCLUSIONS

In summary, the charged black-bounce spacetimes (Eq.1) neatly interpolated between the regular black hole and traversable wormholes, we studied the ringing of the black hole/wormhole transition, which showed that this transition is characterized by echoes and observed three qualitatively distinct types of quasinormal ringdown behaviour:

- (i) the usual ringing of the regular black hole;
- (ii) the remnant of the initial fundamental quasinormal mode, followed by the series of echoes after the black-hole/wormhole transition;
- (iii) the obvious wormhole's mode, after the initial outburs.

This work we considered the scalar and electromagnetic perturbations for the charged black-bounce spacetimes, which showed that the echoes signals of the two perturbations have very similar characteristics. For future work, we

can go further to investigate the gravitational field perturbations[40] for the charged black-bounce spacetimes, and this study based on QNMs may be checked in future gravitational wave plans.

ACKNOWLEDGMENTS

We are very grateful to Dr. Alexander Zhidenko from Brazil for providing me with his mathematica code with the implementation of the Prony method. This research was funded by the National Natural Science Foundation of China (Grant No.11465006).

-
- [1] K. Akiyama et al.(Event Horizon Telescope Collaboration) *Astrophys. J.* **875** L1 (2019).
 - [2] K. Akiyama et al.(Event Horizon Telescope Collaboration) *Astrophys. J.* **875** L2 (2019).
 - [3] K. Akiyama et al.(Event Horizon Telescope Collaboration) *Astrophys. J.* **875** L3 (2019).
 - [4] K. Akiyama et al.(Event Horizon Telescope Collaboration) *Astrophys. J.* **875** L4 (2019).
 - [5] K. Akiyama et al.(Event Horizon Telescope Collaboration) *Astrophys. J.* **875** L5 (2019).
 - [6] K. Akiyama et al.(Event Horizon Telescope Collaboration) *Astrophys. J.* **875** L6 (2019).
 - [7] B. P . Abbott et al. (LIGO Scientific and Virgo), *Phys. Rev. Lett.* **116** 061102 (2016).
 - [8] B. P . Abbott et al. (LIGO Scientific and Virgo), *Astrophys. J. Lett.* **818** L22 (2016).
 - [9] B. P . Abbott et al. (LIGO Scientific and Virgo), *Phys. Rev. X* **6** 041015 (2016).
 - [10] B. P . Abbott et al. (LIGO Scientific and VIRGO),*Phys. Rev. Lett.* **118** 221101 (2017).
 - [11] A. övgün, I. Sakalli, and J. Saavedra, *Chin. Phys. C* **42**, 105102 (2018).
 - [12] D. Du, B. Wang, and R. Su, *Phys. Rev. D* **70**, 064024 (2004).
 - [13] C. Chirenti, *Braz. J. Phys.* **48**, 102 (2018).
 - [14] S. Iyer and C. M. Will, *Phys. Rev. D* **35**, 3621 (1987).
 - [15] R. A. Konoplya, *Phys. Rev. D* **68**, 024018 (2003).
 - [16] M. Saleh, B. Thomas, and T. C. Kofane, *Astrophysics Space Science* **350**, 721 (2014).
 - [17] Poulami Dutta Roy, S. Aneesh and Sayan Kar, *Eur. Phys. J. C* **80**, 850 (2020).
 - [18] H. Liu, P. Liu, Y. Liu, B. Wang and J. P. Wu, *Phys. Rev. D* **103**, 024006 (2021).
 - [19] M. S. Churilova and Z. Stuchlik, *Class. Quant. Grav.***37**, 075014(2020).
 - [20] V. Cardoso and P. Pani, *Nature Astron* **1**, 586 (2017).
 - [21] P. Bueno, P. A. Cano, F. Goelen, T. Hertog and B. Verhocke, *Phys. Rev. D* **97**, 024040(2018).
 - [22] Y. T. Wang, J. Zhang, S. Y. Zhou and Y. S. Piao, *Eur. Phys. J. C* **79**, 726 (2019).
 - [23] M. S. Churilova, R. A. Konoplya and A. Zhidenko, *Phys. Lett. B* **802**, 135207 (2020).
 - [24] C. Vlachos, E. Papantonopoulos and K. Destounis, *Phys. Rev. D* **103**, 044042 (2021).
 - [25] M.S. Churilova, R.A. Konoplya, Z. Stuchlk and A. Zhidenko, *Journal of Cosmology and Astroparticle Physics* **2021**, 10 (2021).
 - [26] Yi Yang, Dong Liu, Zhaoyi Xu, Yujia Xing, Shurui Wu and Zheng-Wen Long, *Phys. Rev. D* **104**,104021 (2021).
 - [27] Dong Liu, Yi Yang, Shurui Wu, Yujia Xing, Zhaoyi Xu and Zheng-Wen Long, *Phys. Rev. D* **104**, 104042 (2021).
 - [28] Edgardo Franzin et al, [arXiv:2104.11376](https://arxiv.org/abs/2104.11376), 2021.
 - [29] Yang Guo et al, [arXiv:2112.01747](https://arxiv.org/abs/2112.01747), 2021.
 - [30] Alex Simpson, [arXiv:2110.05657](https://arxiv.org/abs/2110.05657), 2021
 - [31] M. S. Morris, K. S. Thorne, and U. Yurtsever, *Phys. Rev. Lett.***61**, 1446 (1988).
 - [32] P. Boonserm, T. Ngampitipan, A. Simpson, and M. Visser, *Phys. Rev. D* **98**, 084048 (2018).
 - [33] R.A. Konoplya, A.F. Zinhailo, Z. Stuchlk, *Phys. Rev. D* **99**, 124042 (2019).
 - [34] R.A. Konoplya, C. Posada, Z. Stuchlk, A. Zhidenko, *Phys. Rev. D* **100**, 044027 (2019).
 - [35] R. A. Konoplya, Alexander Zhidenko, *Rev. Mod. Phys.* **83**, 793 (2011).
 - [36] V. Cardoso, E. Franzin and P. Pani, *Phys. Rev. Lett.* **116**, 171101 (2016).
 - [37] V. Cardoso, S. Hopper, C. F. B. Macedo, C. Palenzuela and P. Pani, *Phys. Rev. D* **94**,084031 (2016).
 - [38] R. A. Konoplya, Z. Stuchlk and A. Zhidenko, *Phys. Rev.D* **99**, 024007 (2019).
 - [39] E. Barausse, V. Cardoso and P. Pani, *Phys. Rev. D* **89**, 104059 (2014).
 - [40] R. Dong and D. Stojkovic, *Phys. Rev. D* **103**, 024058 (2021).